The cylinder wake in a magnetic field aligned with the velocity

By J. LAHJOMRI, Ph. CAPÉRAN and A. ALEMANY

Laboratoire des Ecoulements Géophysiques et Industriels, LEGI/IMG, BP 53 X,
38041 Grenoble Cedex, France

We investigate experimentally the up- and downstream flow around an insulating cylinder in a conducting fluid subjected to an aligned magnetic field for low values of the magnetic Reynolds number R_m. For high values of the Alfvén number $\alpha = B_0/U_0(\rho\mu_0)^{\frac{1}{2}}$ the upstream flow is characterized by magnetic and kinematic wakes. In this configuration we have measured, for the first time, the local values of the induced magnetic field. The results were analysed in a confined situation and show that the Oseen number $k = \frac{1}{2}R_m(1-\alpha^2)$ is the main parameter that characterizes the perturbation. In the downstream flow the two fields of perturbations (magnetic and kinetic) are characterized by von Kármán eddies. Our experiments were focused on the evolution of these eddies and show in particular that the critical Reynolds number increases strongly with the intensity of the magnetic field.

1. Introduction

The up- and downstream wakes of a non-conducting cylinder translating in an electrically conducting fluid with a velocity aligned with an external magnetic field can be characterized by three independent parameters:

the Reynolds number $\quad R = U_0 l_0/\nu$,

the magnetic Reynolds number $\quad R_m = U_0 l_0 \mu_0 \sigma$,

the interaction parameter $\quad N = \sigma B_0^2 l_0/\rho U_0$,

from which some other non-dimensional numbers can be deduced that have a great physical influence on the flow configuration, for example:

the Alfvén number $\quad \alpha = B_0/[(\rho\mu_0)^{\frac{1}{2}} U_0] = (N/R_m)^{\frac{1}{2}}$,

the Hartmann number $\quad M = B_0 l_0 (\sigma/\rho\nu)^{\frac{1}{2}} = (NR)^{\frac{1}{2}}$.

The typical scales and physical properties used in these expressions are the magnetic field intensity B_0; the characteristic length of the obstacle and velocity of the flow, l_0 and U_0; and the magnetic permeability μ_0, kinematic viscosity ν, electrical conductivity σ and density ρ of the fluid.

Generally, on the laboratory scale, the magnetic Reynolds number is small and magnetic perturbations can be neglected compared with the applied magnetic field. Consequently it is appropriate to characterize the influence of the magnetic field by the interaction parameter, N, which is the ratio of electromagnetic forces to the inertial forces, and the Alfvén number α, which is ratio of the Alfvén wave velocity to the flow

velocity. For sub-Alfvénic conditions, $\alpha \gg 1$, the propagation of the Alfvén waves upstream of the obstacle generates an upstream wake. On the other hand, in super-Alfvénic conditions, $\alpha \ll 1$, only a downstream wake exists.

The analyses proposed in the literature concerning the wakes generated by three-dimensional obstacles do not take into account boundary-layer separation. This means that only asymptotic conditions have been considered. Thus, two types of situations have been studied. The first concerns the Stokes flow modified by an external magnetic field, in which the Hartmann number, characterizing the ratio of electromagnetic forces to viscous forces, is low. The second type, however, considers very large values of the Hartmann number and interaction parameter, giving quasi-two-dimensional up- and downstream wakes analogous to the Taylor column in rotating flow. It is found that the drag increases according to an $(N/R)^{\frac{1}{2}}$ law for large values of the interaction parameter.

The main theoretical papers on two-dimensional situations (which is the case that we consider here) are Yosinobu (1960) and Tamada (1962). Yosinobu proposes a linearized approach (Oseen approximation) to describe the governing equation which is solved by using a power expansion in terms of R, supposed to be very small. The solution then gives the flow configuration up- and downstream in a sub-Alfvénic or super Alfvénic situation. The drag coefficient decreases very slowly with an increase in the Alfvén number and falls abruptly to zero at $\alpha = 1$. Beyond this value it again returns abruptly to a normal value and then increases with α. Tamada gives a general solution for the vorticity distribution throughout an inviscid fluid. For a low value of the interaction parameter, Tamada considers the flow as a perturbation of the ordinary potential solution. The results are given only for large values of the Alfvén number and show a discontinuity on the flow axis downstream. This disturbance reveals a non-diffusive vortical trail which does not dissipate in inviscid flow. Then to describe the flow far away downstream from the obstacle an Oseen type approximation was also used.

Extending the Oseen approximation to describe inviscid flow near the cylinder, Lahjomri (1989) used the relation between the non-dimensional vorticity ω and the velocity v perpendicular to the flow axis

$$\omega = -Nv. \tag{1}$$

This expression must be considered with some caution because the linear approximation supposes the velocity perturbation to be small compared with velocity U_0 at infinity and this hypothesis is not valid at the vicinity of the obstacle. Nevertheless the tendency should be satisfactorily described. We should then expect that according to (1) the vorticity field, illustrated by figure 1 (a–c), tends to decrease the tangential velocity at the cylinder surface upstream and on the other hand to increase the tangential velocity downstream. It is interesting to note that Horlock (1963) has developed an analogous study between Hele-Shaw flow in a converging channel and MHD flow. Visualization of the flow corresponding to an interaction parameter $N = 4.71$ exhibits the tendency previously described (figure 1 b). We can then conclude that the effect of the magnetic field could be to displace the separation point of the boundary layer in the direction of the flow axis downstream and then to reduce the transverse distance between the two lines of eddies in the von Kármán wake.

The experimental aspects have not been widely studied. The only previous works are those of Maxworthy (1962, 1968) and Yonas (1967) for a sphere moving in the direction of the magnetic field, or by Alhstrom (1963). Maxworthy (1969) and Lake (1971) for the Rankine body. Only three papers have been devoted to a two-
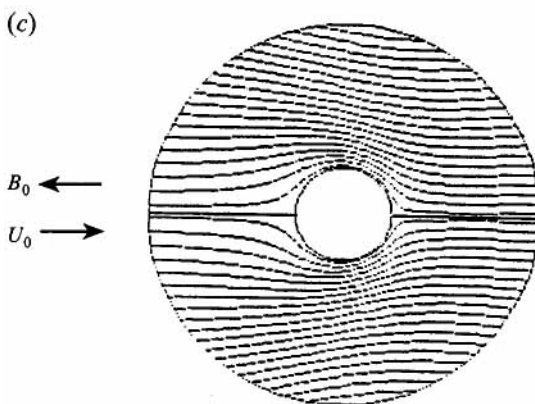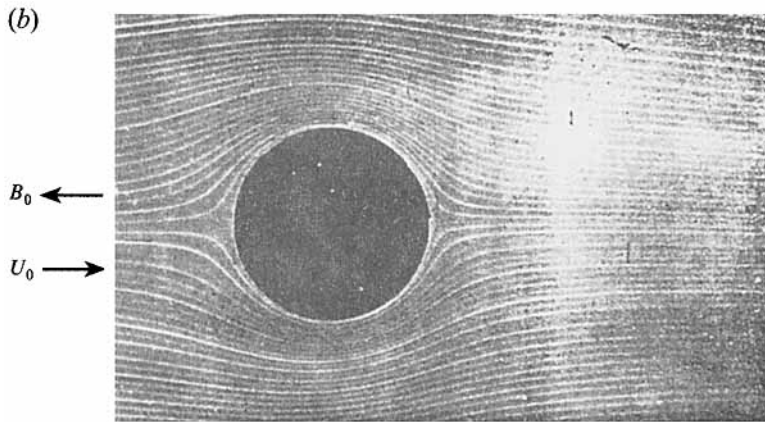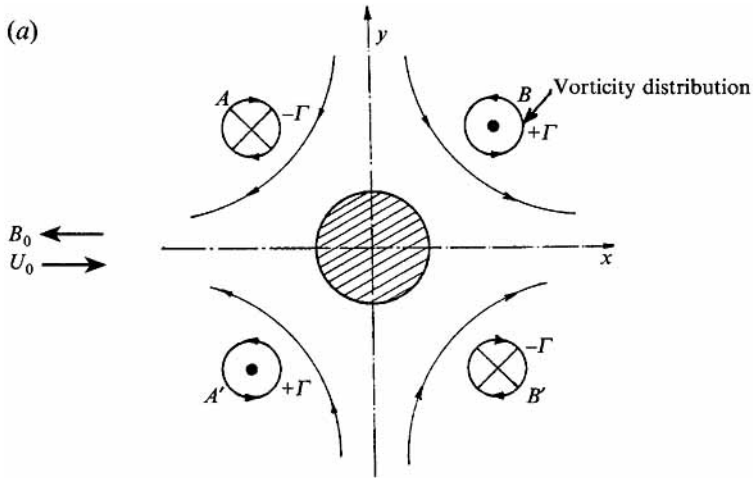
FIGURE 1. (*a*) Schematic distribution of vorticity generated by the electromagnetic forces. (*b*) Analogous experimental MHD flow configuration obtained by a Hele-Shaw flow in a converging channel (Horlock 1963, $N = 4.71$). (*c*) Theoretical flow configuration obtained by a linear Oseen approximation (Lahjomri 1988, $N = 2.4$).

Authors	N	Type of obstacles	Flow configurations	Type of measurements
Maxworthy (1962, 1968)	$\leqslant 1 \geqslant 1$	Sphere	$U_0 \rightarrow$ $B_0 \rightarrow$ ○	Drag pressure distribution and magnetic flux
Ahlstrom (1963)	$\leqslant 1$	Rankine Body	$U_0 \rightarrow$ $B_0 \rightarrow$	Magnetic flux upstream
Yonas (1967)	$\geqslant 1$	Sphere and disc	$U_0 \rightarrow$ ○ $B_0 \rightarrow$	Drag
Maxworthy (1969)	$\leqslant 30$	Rankine Body	$U_0 \rightarrow$ $B_0 \rightarrow$	Pressure distribution and drag
Borisov & Krasilnikove (1981)	$N < 16$	Cylinder	$U_0 \rightarrow$ $B_0 \rightarrow$	Evolution of Strouhal frequency
Golubjev et al. (1984)	$0 < N < 4$	Cylinder	$U_0 \rightarrow$ $B_0 \rightarrow$	Pressure around the body and drag
Josserand et al. (1993)	$0 \leqslant N \leqslant 8$	Cylinder	$U_0 \rightarrow$ $B_0 \rightarrow$	Local pressure measurements and drag
Our study	$\leqslant 1$	Cylinder	$U_0 \rightarrow$ $B_0 \rightarrow$	Local magnetic and velocity field up- and downstream

TABLE 1. Summary of previous experimental studies of the flow around an obstacle in a magnetic field

dimensional obstacle. Borisov & Krasilnikove (1981) were interested in the evolution of the Strouhal number versus the interaction parameter, while Golubjev et al. (1984) were interested in the pressure and drag around a cylinder for moderate values of N. Josserand, Marty & Alemany (1993) have completed this work by measuring local pressure and Strouhal frequency in the boundary layer around the cylinder. All of these studies are summarized in table 1.

The main results of these experimental studies concern the drag coefficient which, according to all the authors increases as $N^{\frac{1}{2}}$ for large values of the interaction parameter. This evolution seems to be due to a decrease of the pressure downstream, the pressure upstream being fixed by its value at the stagnation point.

An interesting observation made by Josserand et al. confirms the tendency already mentioned by Lahjomri and Horlock concerning the displacement of the boundary-layer separation point for moderate values of the interaction parameter. According to this displacement, the low-pressure area downstream from the obstacle and then the drag decrease when N increases from zero to 2.

It appears, finally, that none of the previous works proposes local measurements of velocity and induced magnetic field. The difficulties of performing these local measurements arise because the usual sensors are not sufficiently sensitive to permit a local analysis of the induced field at low magnetic Reynolds numbers.

We propose a local analysis of the flow by using a new type of sensor, the magnetodiode (cf. §2), to measure the local values of the induced magnetic field, hot-film probes being used for the velocity measurements. We are particularly interested in the downstream wake and the possible disappearance of the von Kármán street at some Reynolds number for a fixed value of B_0. One of our objectives is to study the evolution of this critical Reynolds number as a function of the magnetic field.

2. Description of the facility

The experimental installation (figure 2) consists of a large stainless steel container 20 cm in diameter and 2.5 m high, full of mercury. The container is located inside a solenoid that can deliver a uniform magnetic field B_0 continuously adjustable between 0 and 0.4 T. The spatial homogeneity of the magnetic field is about $1/1000$ in a cylinder volume of 10 cm in diameter and 2 m in height.

In this facility, the fluid is at rest and the insulating cylinder moves with a constant velocity U_0 from the top to the bottom of the container. This cylinder is placed on a support on which are also fixed the sensors. This support is connected to a big load which assures the penetration in the mercury. A special device including a motor, supplied with a constant current, controls the velocity of the support with a precision greater than 1% in a range from 0 to 1 m/s. The kinetic or magnetic probes can be placed at any spatial position upstream or downstream from the cylinder, and are connected to various pieces of apparatus used to process the signal, including a computer.

The perturbations of the velocity are measured by hot-film probes (TSI) and the induced magnetic field by the magnetodiodes. These sensors have been tested and analysed by Christoloveanu (1981) and used here in MHD flow for the first time. They consist of a semiconductor bar with two doped junctions (figure 3). We need only to note that the internal resistance of the probe changes when it is submitted to the influence of a magnetic field. Then, if it is supplied by a constant current ($\sim$ 10 mA) the variation of the voltage gives the value of the local magnetic field via a calibration curve (figure 4a). The slope of this curve gives the sensitivity of the sensor, which is a function of the magnetic field intensity and is of order 2.5 mV/Gauss for a mean magnetic field in the range of 0.2 to 0.4 T. In our experiment the spatial resolution of our handmade probe was approximately 1 mm³.

The usable frequency range of this sensor is large ($\sim$ 10 kHz) but is limited at low frequency by the noise of the probe itself, the power spectrum of which behaves as $1/f$ (figure 4b). Nevertheless, it is possible to suppress this disadvantage by subtracting the known noise spectrum from the signal. It is also noticeable that this type of sensor is sensitive to temperature and light. These last two influences can strongly change the signal. Nevertheless, we have not analysed these aspects precisely as they are not really important in our experiment. It is clear that there is no possibility of the sensor being submitted to light when it is immersed in mercury and on the other hand the temperature evolution of the big quantity of liquid metal in the vertical container (1.3 tonnes) is very slow and is quasi-homogeneous at a fixed time due to the excellent thermal conductivity of the mercury.

The influence of the noise of the probe at frequencies lower to 1 Hz is very small and
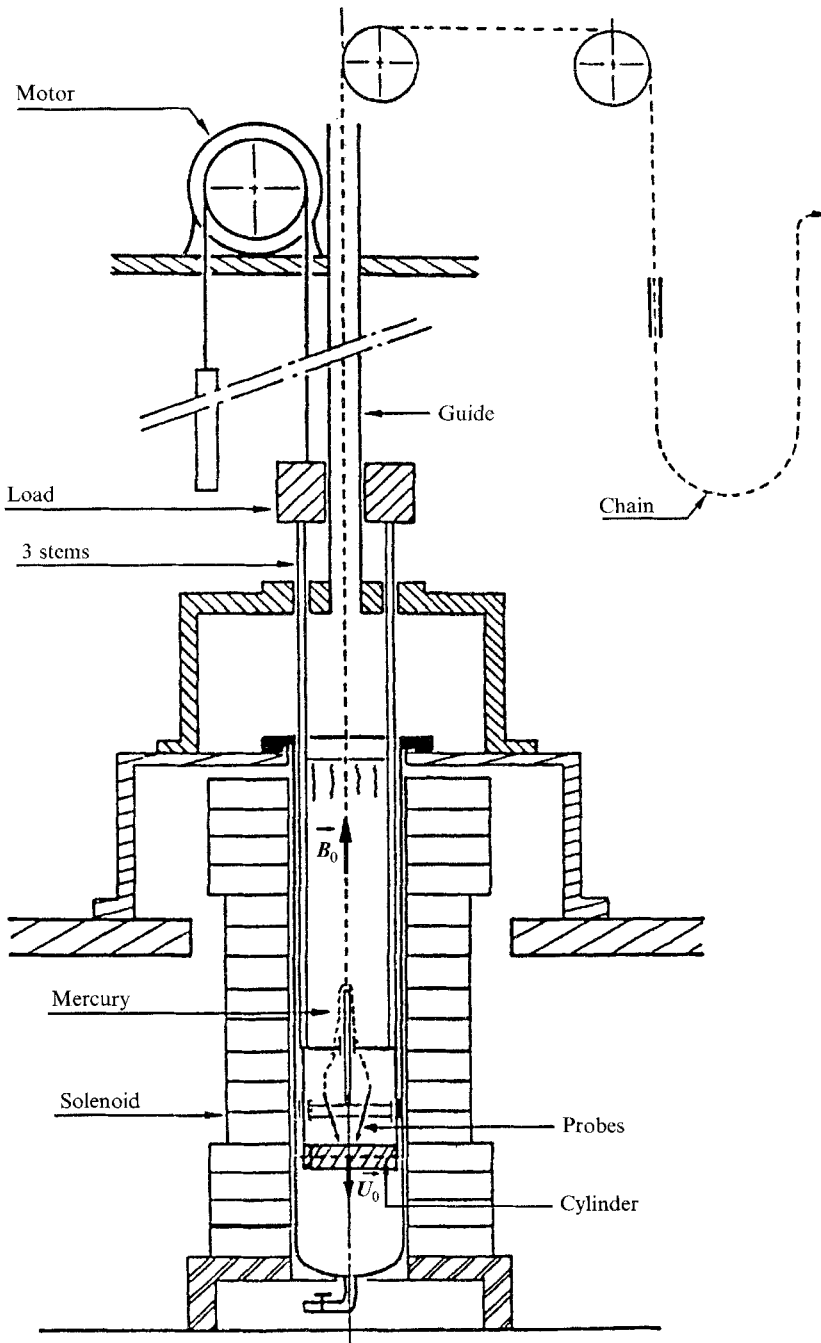
FIGURE 2. Experimental facility.

according to figure 4(*b*) can be evaluated as 4×10^{-3} Gauss. Then the precision of measurements when the flow is stationary is very good. The maximum value of the noise when the frequency increases reaches 1 m/V without any correction, corresponding to 0.2–0.4 Gauss in our experimental conditions. We can then conclude that the maximum value of the error is of order 0.3 Gauss when the flow is fluctuating.
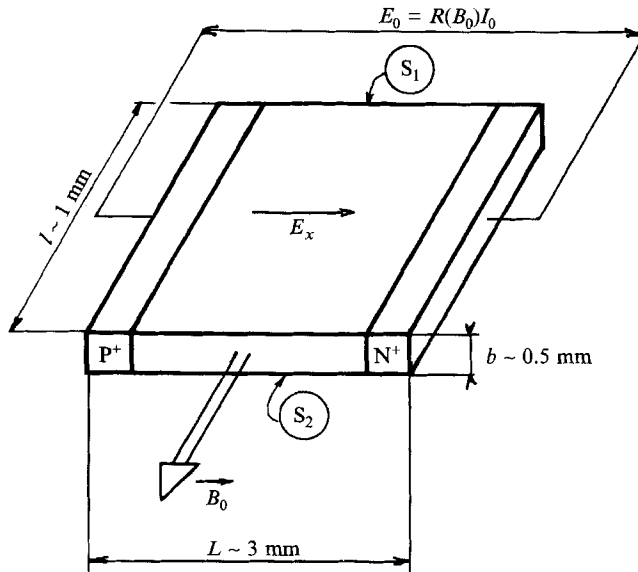
FIGURE 3. Schematic picture of the magnetic sensor: the magnetodiode. For an imposed current, I_0, the voltage, E_0, depends on the apparent resistance, $R(B_0)$, of the probe.

The calibration of the hot-film probes and the magnetodiodes was done in the facility itself, and thus could be checked on site while doing the measurements and could be verified at any time. In this way, we expect good reliability for our data.

The principle of the measurements and the data acquisition system depends on the up- or downstream position of sensors. The upstream flow is steady and the induced magnetic field (which is not fluctuating) must be distinguished from the value of the applied magnetic field. The difficulty comes from the fact that the induced magnetic field at low R_m has the same order of magnitude as the small spatial inhomogeneities of the applied magnetic field. To measure this steady induced magnetic field, we recorded the probe signal while the cylinder was stopped at a given point at mid-level. Thus the value of the induced field was obtained from the instantaneous difference between the probe signal level while running and while at rest. Each data point corresponds to the mean value resulting from ten analogous experiments. This gives us the induced magnetic field upstream from the obstacle.

Under the conditions of the downstream flow corresponding to the formation of a von Kármán street the signals from both the velocity and induced magnetic field are fluctuating. To analyse the two fields of perturbation (magnetic and kinetic) we used filters to suppress the continuous part of the signals. The filter parameters used to process both signals were rigorously the same, in order to obtain an exact phase difference between them. We used an integrator voltmeter to get the r.m.s. and the spectral analysis was performed on a computer.

3. Experimental results

3.1. *Upstream flow*

3.1.1. *Generalities and theoretical aspects*

The range of non-dimensional parameters was chosen in order to generate a sub-Alfvénic flow characterized by high values of the Alfvén number α. These conditions correspond to the formation of an upstream wake which can be also observed in the
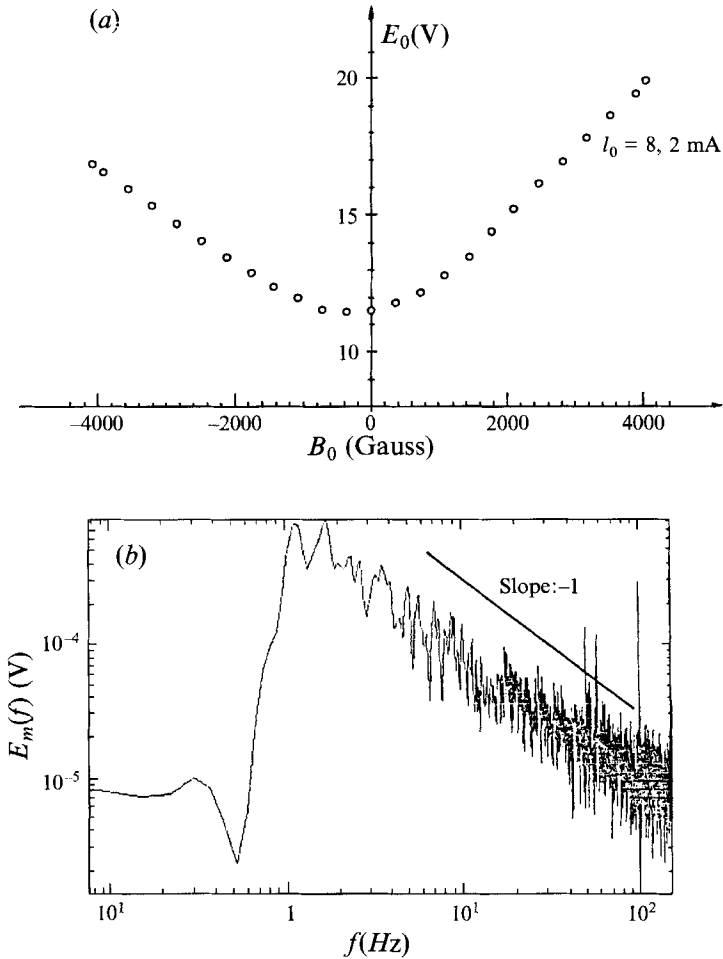
FIGURE 4. (a) Calibration curve of the magnetodiode for $I_0 = 8.2$ mA. (b) Power spectrum of the noise of the magnetodiode.

rotating flow submitted to the Coriolis force or in a stratified flow submitted to a buoyancy force. In each of these situations an external field of forces leads to the flow becoming two-dimensional. We were interested in measuring the induced magnetic field in this wake. The experimental conditions are summarized in table 2, and correspond to an insulating cylinder of diameter $d = 6$ cm and of length 19.8 cm.

Owing to the size of the cylinder ($d = 6$ cm) compared to the size of the container (diameter 20 cm) the confinement or blockage ratio is not negligible. The influence of the confinement has been already taken into account by Ahlstrom (1963) for a Rankine body and Yonas (1967) for a sphere or disc. Yonas has shown that for moderate values of the interaction parameter, the confinement effect results in an increase in the effective velocity which should be used. To take into account this effect when a sphere of diameter d is placed in the centre of a duct of diameter D, Yonas proposed a drag coefficient in the form

$$C_D \approx [1-(d/D)^2]^{-\frac{3}{2}} N^{\frac{1}{2}}$$

and noted than for $N > 10$ the effect of the confinement disappears and an extrapolation of d/D to zero gives

$$C_D = 0.33 N^{\frac{1}{2}}.$$

	Kinetic Reynolds number	Magnetic Reynolds number	Alfvén number	Magnetic Oseen number	Stuart number or interaction parameter
Non-dimensional parameters	$R = \dfrac{U_0 d}{\nu}$	$R_m = \mu_0 \sigma U_0 d$	$\alpha = \dfrac{B_0}{(\rho\mu_0)^{\frac{1}{2}} U_0}$	$k = \frac{1}{2} R_m (1 - \alpha^2)$	$N = \dfrac{\sigma B_0^2 d}{\rho U_0}$
Minimum values	5.2×10^4	6×10^{-3}	7	-1.8	0.6
Maximum values	20.8×10^4	28×10^{-3}	22	-0.566	3.6

TABLE 2. Experimental conditions

This implies that for this range of interaction parameter the wake spreads so slowly that it does not interact with the walls.

Ahlstrom (1963) used a linear theory to calculate the decay rates of the magnetic field in the upstream wake by taking into account the influence of the walls, supposed perfectly conducting. The theory established for a Rankine body was compared with experiment and showed a good agreement. The main results revealed that, due to the confinement effect, the induced magnetic field follows an exponential decay instead of decreasing inversely as the distance from the obstacle, as for an infinite medium.

We propose to evaluate the importance of this effect in our facility by modelling the real boundary conditions which are not two-dimensional (and very difficult to analyse) by a simpler model where the circular wall of the container is replaced by two plane walls parallel to the cylinder axis. Neglecting the viscosity, and linearizing the equations (the Oseen magnetic approximation) we obtain

$$\omega = -\frac{B_0}{\rho U_0} j, \quad \frac{2k}{d}\frac{\partial \omega}{\partial x} = \nabla^2 \omega, \quad k = \frac{1}{2} R_m (1 - \alpha^2). \tag{2}$$

The coordinate x corresponds to the direction of the mean velocity and magnetic field, z is the axial direction of the cylinder, y completes the coordinate system, and ω and J are the vorticity and current density respectively. The Oseen number k is negative for high values of the Alfvén number, that is to say, for large values of the magnetic field.

Using the stream functions ϕ and ψ for the velocity u ($u = \delta\phi/\delta y$, $v = -\delta\phi/\delta x$) and magnetic field b ($b_x = \delta\psi/\delta y$, $b_y = -\delta\psi/\delta x$) fluctuations, (2) is converted to

$$\frac{\nabla^2 \phi}{U_0} = -\alpha^2 \frac{\nabla^2 \psi}{B_0}, \tag{3}$$

$$\frac{2k}{d}\frac{\partial \nabla^2 \phi}{\partial x} = \nabla^4 \phi. \tag{4}$$

The solution can be expressed as the sum of a series of functions:

$$\left. \begin{aligned} \phi &= -U_0 d\alpha^2 \left[\sum_n A_n \sin\left(\lambda_{1n}\frac{y}{d}\right) \exp\left[-k \pm (k^2 + \lambda_{1n}^2)^{\frac{1}{2}}\frac{x}{d} \right] - \sum_n B_n \sin\left(\lambda_{2n}\frac{y}{d}\right) e^{\pm \lambda_{2n} x/d} \right], \\ \psi &= B_0 d \left[\sum_n A_n \sin\left(\lambda_{1n}\frac{y}{d}\right) \exp\left[k \pm (k^2 + \lambda_{1n}^2)^{\frac{1}{2}}\frac{x}{d} \right] + \sum_n B_n \sin\left(\lambda_{2n}\frac{y}{d}\right) e^{\pm \lambda_{2n} x/d} \right]. \end{aligned} \right\} \tag{5}$$
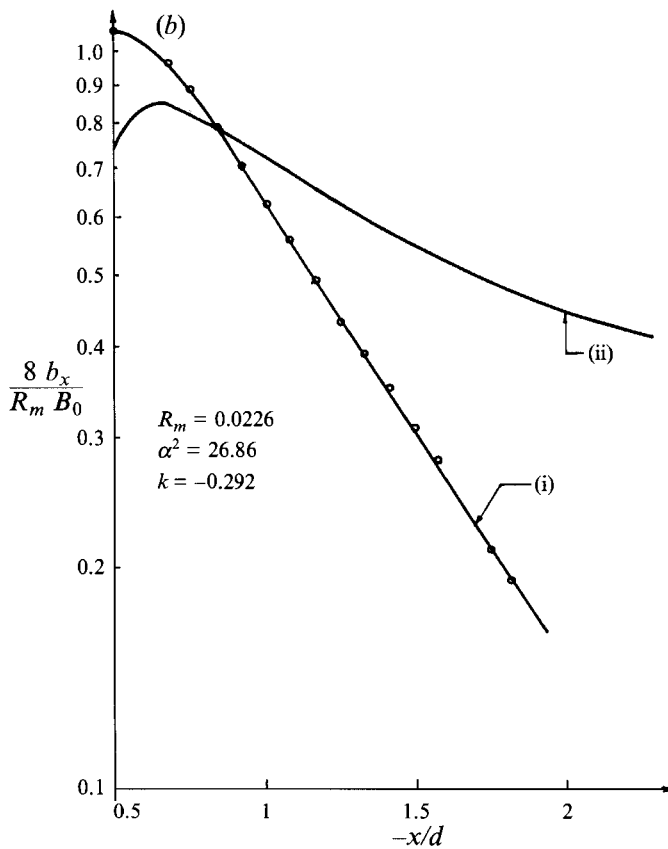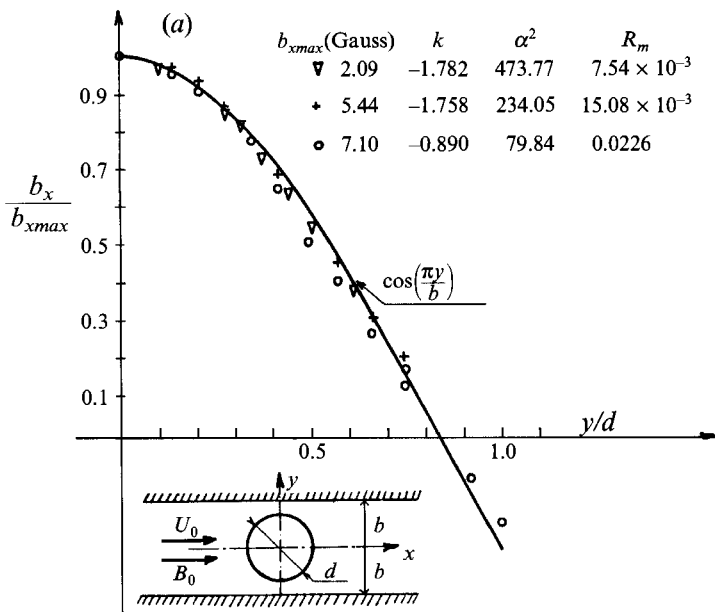
FIGURE 5. (a) Non-dimensional induced magnetic field profile in a cross-section located at 1 diameter from the cylinder. (b) Experimental decay of the magnetic perturbation compared with the unbounded theory (i) experimental results, (ii) theoretical results.

The signs $+$ or $-$ respectively denote $x < 0$ or $x > 0$. The values of λ_{1n} and λ_{2n} are determined by the boundary conditions. The two planes $y = \pm b$ must be streamlines ($v_y = 0$), and if we suppose that the walls are perfectly conducting, the two planes $y = \pm b$ are also magnetic lines ($b_y = 0$). These two conditions allow us to deduce the values of the parameters λ_{1n} and λ_{2n}:

$$\lambda_{1n} = \lambda_{2n} = n\pi d/b \quad (n \text{ integer}). \tag{6}$$

Without considering more detailed theoretical aspects we can predict the decay rate (η) of the perturbation in the upstream wake by taking into account only the first-order term of the development, for $x/d \geqslant 1$ and $k \sim -\lambda_1$ (corresponding to experimental conditions):

$$\eta = k + (k^2 + \pi^2 d^2/b^2)^{\frac{1}{2}}. \tag{7}$$

In the same way, the shape of the non-dimensional induced magnetic field profile is

$$b_x/b_{x(\max)} \approx \cos(\pi y/b) \tag{8}$$

for the axial component.

We note that for the very high values of the magnetic field, $k \ll 1$, the decay rate of the perturbation becomes independent of the confinement ratio and tends to zero. For that condition we find a quasi-two-dimensional wake (as already pointed out by Yonas and others) independent of the electrical conductivities of the walls.

3.1.2. *Interpretation of the measurements*

The measurements concern both the induced magnetic field profiles in a cross-section and the evolution of the field intensity in the axial direction. We observe in figure 5(*a*) that the shape of the profile obtained for a blockage ratio $d/2b = 0.3$ and for different values of the Oseen and Alfvén numbers agrees very well with the one given by (8). Our measurements were limited to a distance of two radii from the obstacle which corresponds to the limits of the displacement for our support.

We have plotted on figure 5(*b*) the evolution of the induced magnetic field as predicted by the theory in the unbounded case, and the experimental evolution for the same value of the central parameters (the value of b_x is normalized by its maximum theoretical value $\frac{1}{8}R_m B_0$). We see that the experimental decay follows the exponential law already observed by Ahlstrom (1963) for a Rankine body (unlike the unbounded theory which gives a power law decay). These results are confirmed by the measurements of the decay rate of the perturbation versus the Oseen number when compared with the previous theory and equation (7) (figure 6*a*). We note that a very good agreement between the experimental and theoretical results and the small difference between them could be due to the simplified geometry which we have used in our model. On the other hand, it is obvious that for a given blockage ratio the evolution of the perturbation depends only on the value of the Oseen number. We can confirm this observation by plotting the normalized values of the perturbation field for various values of the Reynolds number, magnetic Reynolds number and Alfvén number but for a fixed value of the Oseen number (figure 6*b*). We see that all the experimental points can be regrouped on a single curve, according to the theoretical aspect in unbounded or confined theory. The small difference which appears between curves (i), (iii) and curve (ii) can be explained by experimental imprecision (cf. figure 7 where the location of the points (i), (ii), (iii) in $(b/B_0, R_m)$-space are shown). The evolution of the magnetic field intensity of the perturbations on the x-axis of the flow versus the magnetic Reynolds number differs slightly from the theoretical unbounded case (figure 7).
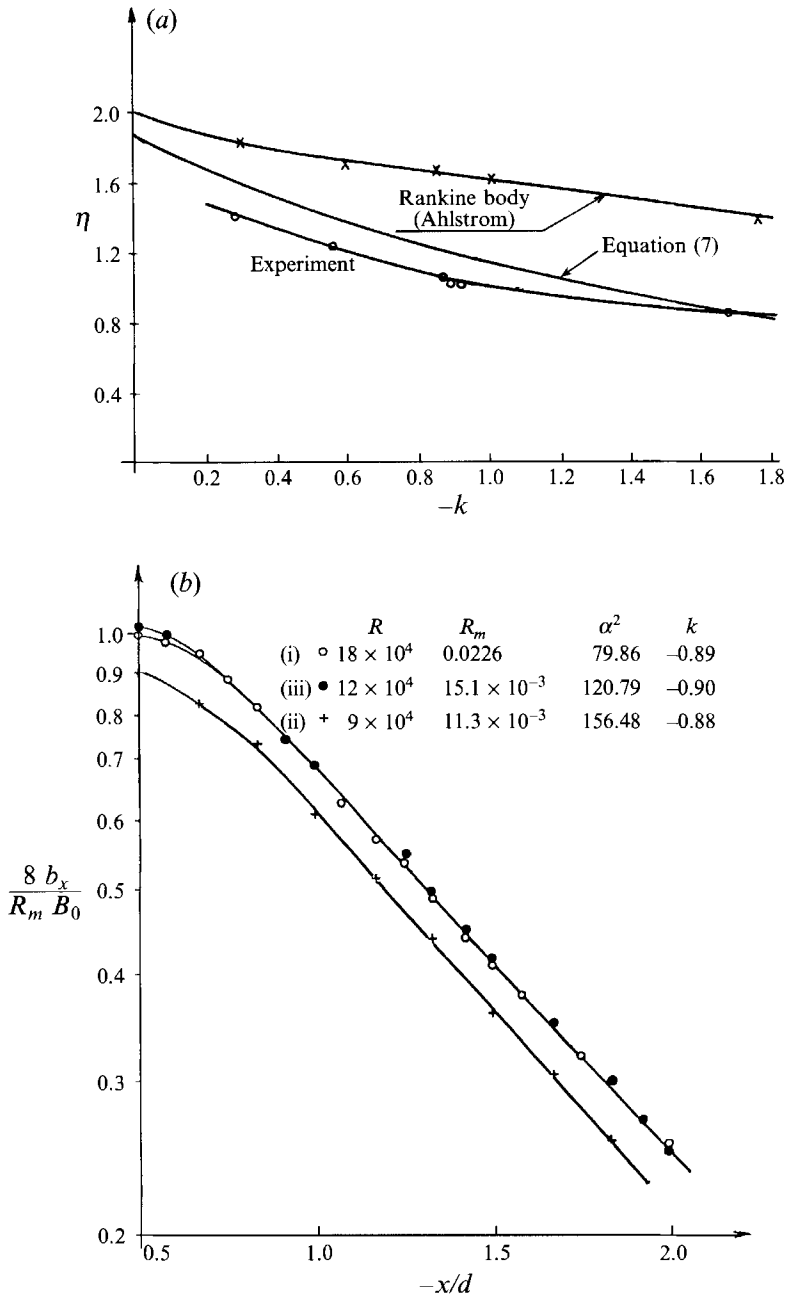
FIGURE 6. (a) Decay rate of the magnetic perturbation compared with the Oseen approximation theory. (b) Universal decay of the magnetic perturbation versus the distance from the cylinder, for a given value of the Oseen number.

3.2. Flow configuration downstream from the cylinder

3.2.1. Generalities

In this part of our study, the flow is generated by an insulating cylinder 1 cm in diameter producing a blockage ratio (d/D) of 0.05, much smaller than that for the upstream flow. The other non-dimensional physical parameters using the diameter of
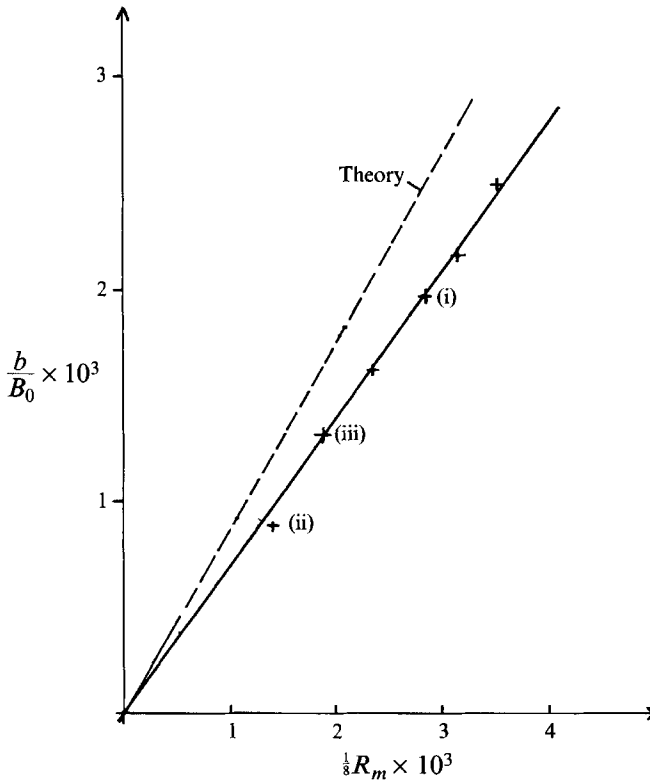
FIGURE 7. Evolution of the normalized induced magnetic field versus the magnetic Reynolds number, $x/d = -1$, $y/d = 0$, $k = -0.88$.

	Kinetic Reynolds number	Magnetic Reynolds number	Alfvén number	Stuart number or interaction parameter	Hartmann number
Non-dimensional parameters	$R = \dfrac{U_0 d}{\nu}$	$R_m = \mu_0 \sigma U_0 d$	$\alpha = \dfrac{B_0}{(\rho\mu_0)^{\frac{1}{2}} U_0}$	$N = \dfrac{\sigma B_0 d}{\rho U_0}$	$M = \left(\dfrac{\sigma}{\rho\nu}\right)^{\frac{1}{2}} B_0 d$
Minimal values	10^3	2.5×10^{-3}	0	0	0
Maximal values	4×10^4	6×10^{-3}	21	0.81	10^3

TABLE 3. Parameters for the experiments on the flow downstream of the cylinder

the cylinder as typical scale are given in table 3. We can conclude from this table that the Reynolds number is very high and thus the viscous forces are generally negligible except in the boundary layer on the cylinder. The magnetic Reynolds number is very low and consequently the induced magnetic field will be small. On the other hand the electromagnetic forces are strong compared with the viscous forces, i.e. the Hartmann number is high. Measurements have been taken in both a sub-Alfvénic and a super-Alfvénic regime.

3.2.2. *Flow configurations*

It is well known that, without a magnetic field, the wake of a two-dimensional cylinder is characterized by von Kármán street eddies, if the Reynolds number is higher than a critical value close to 40. The electromagnetic forces resulting from the action
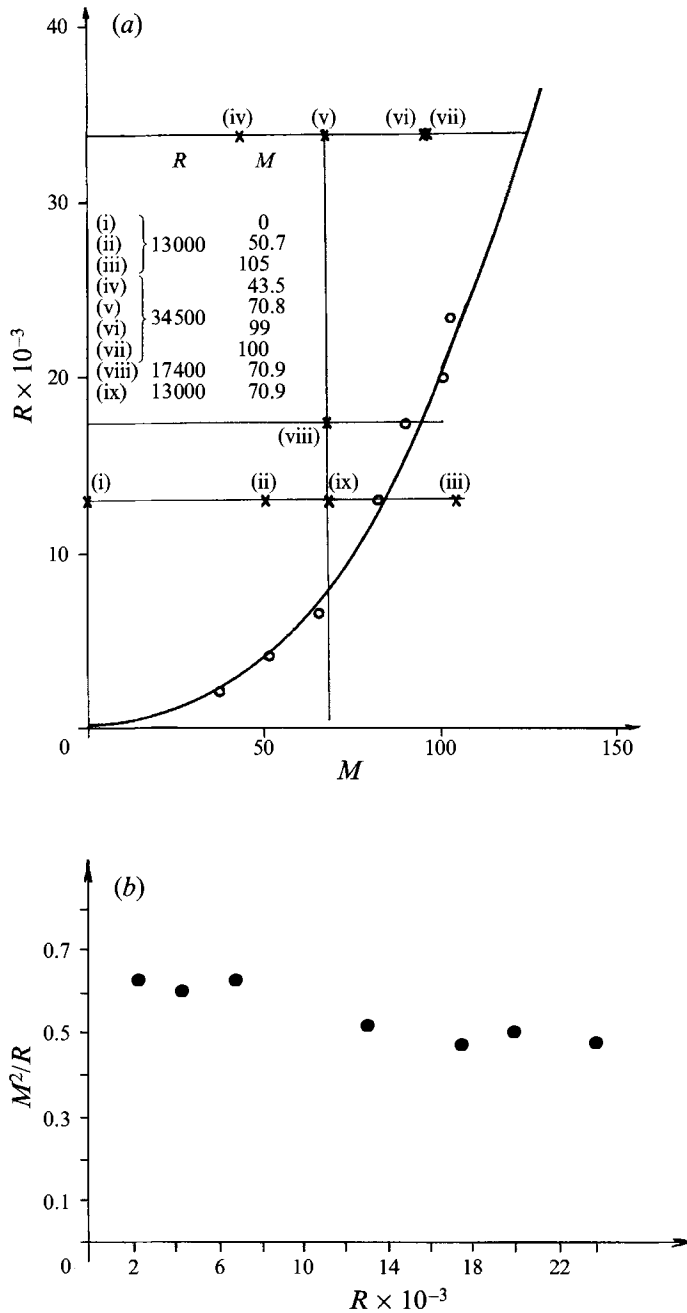
FIGURE 8. (a) Evolution of the critical Reynolds number versus the Hartmann number, $x/d = 2.5$, $y/d = 0.8$. (b) The existence of a critical value of the interaction parameter in the range of parameters used.

of a longitudinal magnetic field are able to stabilize the flow and then to delay the appearance of the von Kármán eddies, which occur at a much higher value of the Reynolds number when the applied magnetic field increases. This phenomenon was experimentally observed by Borisov & Krasilnikove (1981) in a geometrical

configuration similar to this study and by Maxworthy (1962) who noted the disappearance of vortex shedding behind a sphere.

We were interested to confirm experimentally this possible transition by analysing the signals given by hot-film probes (for the velocity fluctuations) and by the magnetodiodes (for the induced magnetic field). For a fixed Reynolds number, low values of the Hartmann number correspond to the formation of a von Kármán vortex street which then disappears when the Hartmann number becomes greater than a critical value. The critical curve (figure 8 a) separating the domains of existence or non-existence of the von Kármán vortex street in the (M, R)-plane obtained experimentally, corresponds to a Reynolds number ranging from 0 to about 35000 and a Hartmann number from 0 to 105.

Each point on the curve results from the same simple procedure, which consists of noting the disappearance of the Strouhal frequency in the spectrum of the magnetic field when the Hartmann number increases (for a fixed value of the Reynolds number). The characterization of the minimum value of the root mean square of the filtered bandpass signal corresponds to the critical Hartmann number. The average value of the results corresponding to five identical procedures gives one point of the critical curve. This gives a quasi-constant value of the transition interaction parameter M^2/R close to 0.55 (figure 8 b). This value is very close to the experimental results found by Maxworthy (1962) for the wake of a sphere ($N = 0.5$), but is very far from the experimental criterion proposed by Borisov & Krasilnikove (1981) which gives the transition for a value of M/R equal to 0.034. This very important difference in the transition criterion is difficult to analyse, the paper of Borisov & Krasilnikove being very short (two pages) and published in Russian. We can note only that their experimental method used a heat source placed within the cylinder, the measurements of thermal perturbations in the wake being taken by thermoelements in a range of parameters approximately the same as in the present paper; but contrary to our experiment, the cylinder is fixed and is placed in an external flow of liquid metal. Then the control of the flow conditions is not as good as in our facility, the measurement technique adopted for the velocity fluctuations is not very sensitive and the results were not confirmed by the induced magnetic field measurements. Finally we have done many experiments in the region where, according to Borisov & Krasilnikove, the von Kármán eddies should be present and we have not observed Strouhal fluctuations. Most of the experimental results referred to in the following text we have studied at points (i) to (ix).

Some samples of the velocity and magnetic field signals at points (i), (ii) and (iii) located 2.5 diameters behind the cylinder are given on figure 9. For $B_0 = 0$, the magnetodiode signal corresponds to the sensor noise, while the velocity signal shows oscillations typical of the von Kármán street. At point (ii) ($R = 13000$, $M = 50$) there appears to be a correlation between the magnetic and velocity oscillations. One notes that some turbulence exists on the axis of the flow which decreases when y/d increases. At point (iii) which is outside the von Kármán street domain, only some turbulence seems to be maintained.

It is easy to measure the frequency f of the von Kármán oscillations by measuring the time corresponding to 10 periods of magnetic and kinetic fluctuations. This time can be very precisely found by using a storage oscilloscope. We can then calculate the Strouhal number

$$S = fd/U_0$$

and its evolution with the magnetic field. According to figure 10, this evolution seems to be a function of the interaction parameter only. For a zero magnetic field, its
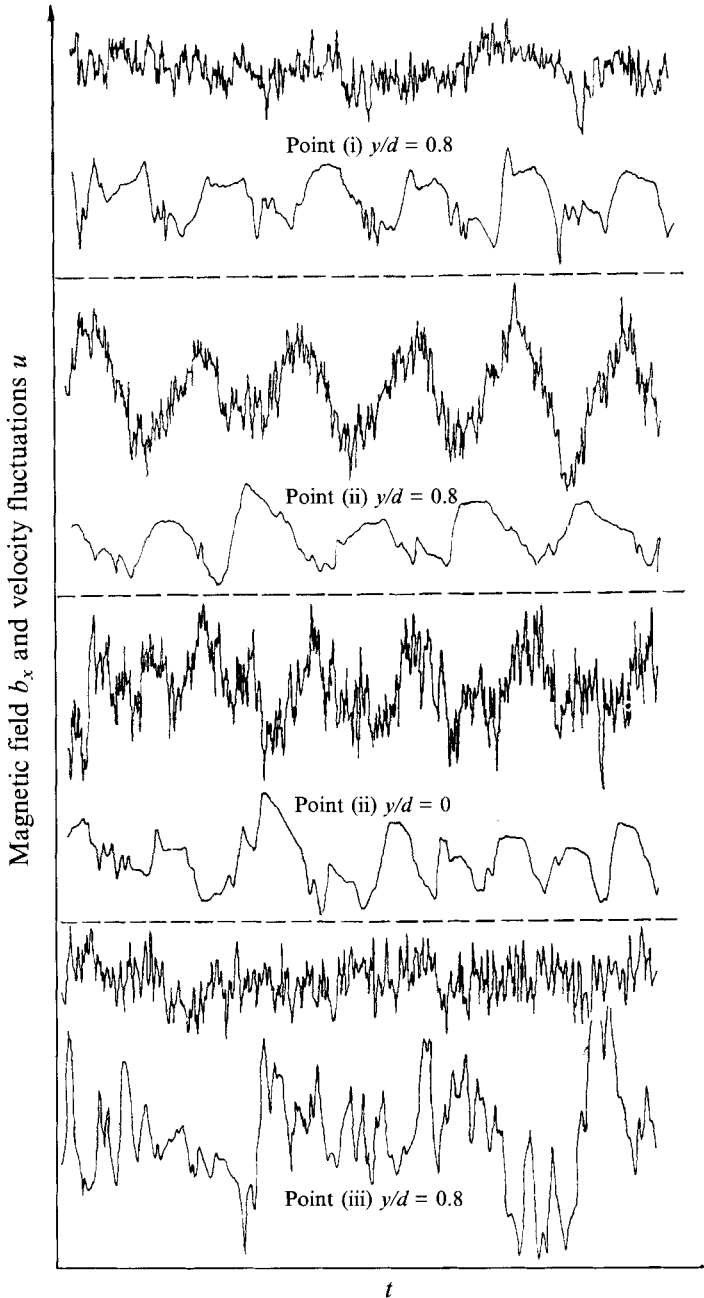
FIGURE 9. Velocity u (lower curves) and induced magnetic signals b_x (upper curves) at three typical points (i, ii, iii) located at a distance $x/d = 2.5$ from the cylinder.

classical value (Roshko 1954) is equal to 0.22 far from the flow axis (and reaches 0.44 on the axis where the influence of the two streets can be felt). We obtain a slightly greater value ($S = 0.25$ for $N = 0$) for a distance $y/d = 0.8$ from the flow axis. The decay of S when N increases could be explained by the fact that, due to the Joule effect, the increase in the size of each eddy that forms on the cylinder is lower than without
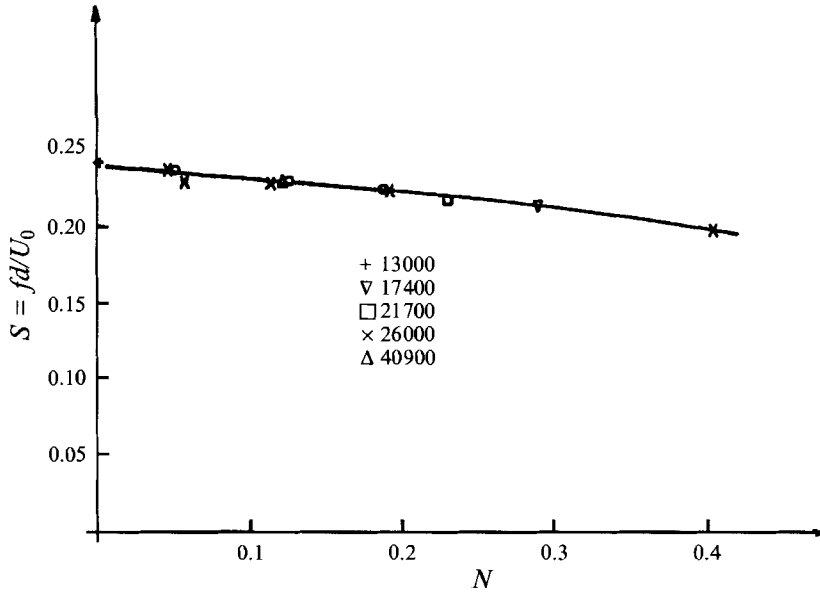
FIGURE 10. Evolution of the Strouhal number with the interaction parameter.

a magnetic field. It follows that the extraction of each eddy by the external flow is delayed. This also means that, according to Shercliff (1965), one of the effects of a DC magnetic field is to reduce the vorticity. We can note that the decay of S is relatively low, and after a value of N near 0.5 the von Kármán eddies suddenly disappear.

The phase relationship between magnetic and kinetic fluctuations depends on the distance y/d from the flow axis. When this distance is greater than the typical interval between the two eddy streets, the flow is not very sensitive to the alternate distribution of the eddies. Therefore the phase displacement between the magnetic and kinetic structures remains constant. On the other hand, near the flow axis the magnetic field distribution is strongly dependent on the spatial distribution of eddies. This distribution of the induced magnetic field is governed by a classical diffusion convection equation (induction equation). The importance of the convection effect can be appreciated through the magnetic Reynolds number ratio of a typical time of diffusion to a typical time of convection. When the magnetic Reynolds number is low, the convection effect is low but is not zero. This effect is more sensitive within the high-velocity region than outside it. Therefore, the tendency of the flow to distort the magnetic lines in the direction of the velocity field is more sensitive in the vicinity of the axis of the eddy street. This explains the magnetic lines distribution close to the flow axis (see the schematic representation on figure 11).

Some theoretical treatment of the magnitude and evolution of the phase displacement between magnetic and kinetic fields of structures can be also given. Consider the component of the induction equation in the direction of the x-axis:

$$\frac{\partial^2 b_x}{\partial x^2} + \frac{\partial^2 b_x}{\partial y^2} = -\mu_0\, \sigma \left(b_y \frac{\partial U_0}{\partial y} - U_0 \frac{\partial b_y}{\partial y} + B_0 \frac{\partial u}{\partial x} - \frac{\partial b_x}{\partial t} \right), \tag{9}$$

where the velocity V and magnetic field B are the sum of a mean part and fluctuating part:

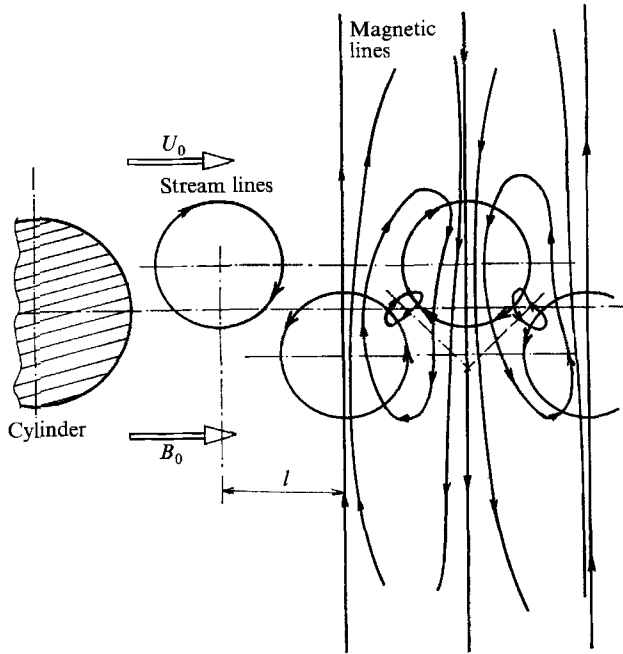$$V = U_0 + u, v, \quad B = B_0 + b_x, b_y, \tag{10}$$

FIGURE 11. Schematic representation of both streamlines and induced
magnetic lines in a von Kármán street.

and where u and v are of the same order of magnitude as $U_0(y)$ when b_x and b_y are of
the order of $R_m B_0$. Then the induction equation can be reduced to

$$\frac{\partial^2 b_x}{\partial x^2} + \frac{\partial^2 b_y}{\partial y^2} = -\mu_0 \sigma B_0 \frac{\partial u}{\partial x}. \tag{11}$$

If we suppose u and b_x respectively in the form

$$\left. \begin{aligned} u &= f(y)\,\mathrm{e}^{\mathrm{i}(kx+\omega t)}, \\ bx &= g(y)\,\mathrm{e}^{\mathrm{i}(kx+\omega t+\phi(y))}, \end{aligned} \right\} \tag{12}$$

we obtain from (11)

$$\mathrm{e}^{\mathrm{i}(\phi+\pi/2)}(2g'\phi' + g\phi'') + \mathrm{e}^{\mathrm{i}\phi}(g'' - g\phi'^2 - k^2 g) = k\mu_0 \sigma B_0 f\mathrm{e}^{\mathrm{i}\pi/2}. \tag{13}$$

Far from the flow axis, the phase displacement can be considered as independent of
y ($\phi(y) = $ constant) and the solution of (13) gives immediately

$$\phi = \tfrac{1}{2}\pi.$$

The experimental values of the phase relationship were easy to deduce by recording
both the magnetic and kinetic signals and by measuring their time displacement. The
results correspond to an average value from 10 periods, the calculation being made
using the formula

$$\phi = 2\pi \,\Delta t/T,$$

where Δt represents the time displacement between the two signals (magnetic and
kinetic) and T their period. The computer calculation gives the results shown in figure
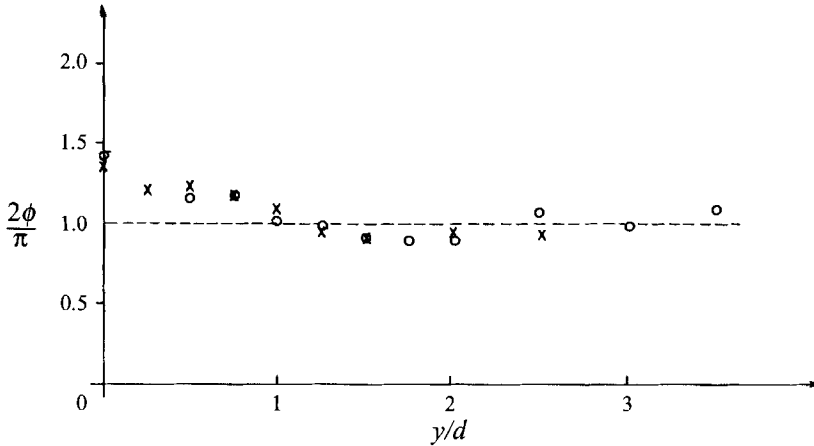
FIGURE 12. Phase displacement between velocity and induced magnetic field fluctuations versus the transverse distance, y/d, of the mean flow; $x/d = 2.5$.

12 and shows a phase displacement near $\frac{1}{2}\pi$ far from the axis, according to the theoretical prediction. We observe an increase of ϕ, when the distance from the flow axis decreases, which reaches the value $\pi/1.38$ when $y/d = 0$.

3.2.2. *Magnetic and kinetic energy profiles*

The previous paragraph was devoted to the evolution of the critical Reynolds number which characterizes the disappearance of the von Kármán eddy street when the Hartmann number increases. The existence of magnetic eddy lines connected with the two lines of kinetic eddies had been experimentally verified (and measured for the first time), the axial magnetic fluctuation having the Strouhal frequency. The analysis proposed in the following concerns the configuration of the weak, both magnetic and kinetic, relationship between these two fields of fluctuations and their evolution with the applied magnetic field.

The mean-square value of the magnetic and kinetic fluctuations $\langle b_x^2 \rangle$ and $\langle u^2 \rangle$ corresponds to the sum of the von Kármán eddies and some turbulence contained in the range of frequency of our bandpass signal (about 20 Hz around the von Kármán frequency); in most cases the turbulence intensity was lower than the von Kármán eddy intensity. The values obtained depend on three parameters: the Hartmann number, the Reynolds number and the distance from the cylinder. For a fixed value of the non-dimensional distance from the cylinder, $x/d = 2.5$, the profile of kinetic energy for the velocity fluctuations depends, then, only on M and R or two combinations of these parameters. Figure 13(a) represents the transverse profiles plotted for the conditions corresponding to points (i), (ii), (iii) and (iv) on figure 8(a). We note a narrowing of the profiles at $y/d = 0.5$ when M increases and at the same time the total energy decreases. This phenomena is particularly sensitive at the point (iii) which is outside the von Kármán region. This configuration is very different from the others and seems to correspond to the formation of a local discontinuity of the mean velocity located near the line $y/d = 0.5$ (the edge of the cylinder). For a fixed value of M the energy increases (in the von Kármán region) when R increases. At $y/d = 0$, the velocity peak is due to the addition of the influence of the two lines of eddies and some turbulence. The turbulence level is higher within the von Kármán region than outside, because the eddies supply the turbulence as a forcing at a fixed wavenumber corresponding to the local value of the Strouhal number. The turbulence level seems
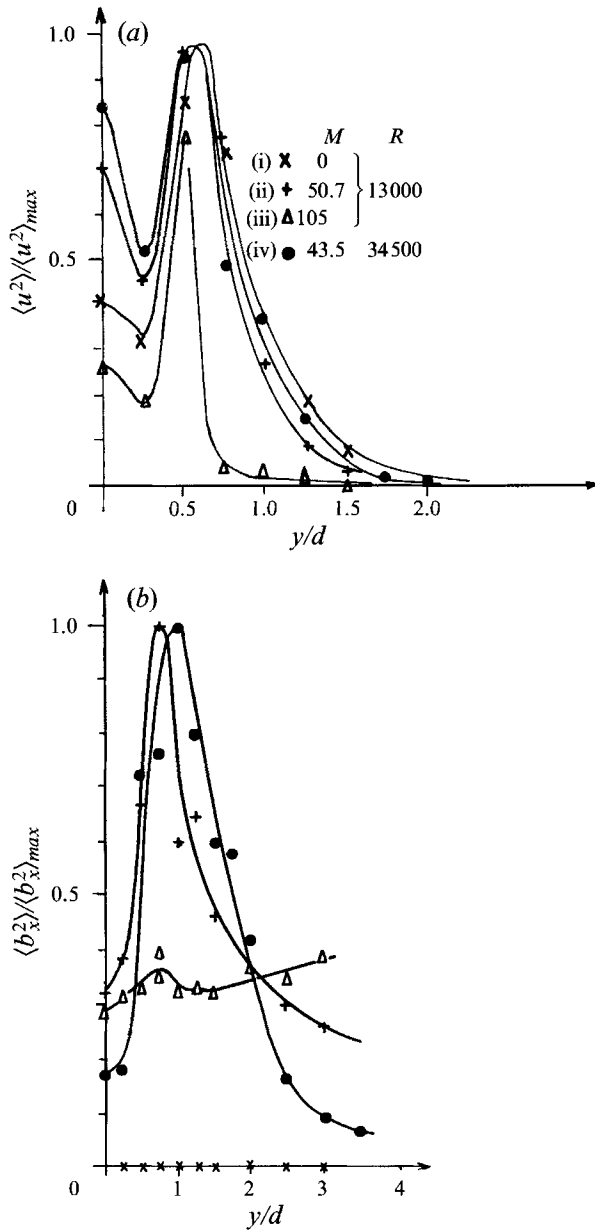
FIGURE 13. (a) Kinetic energy profiles and (b) magnetic energy profiles in a cross-section located at 2.5 diameters from the cylinder. The values for curve (iii) (magnetic energy) are normalized by the maximum value of curve (ii).

to be higher on the velocity signal than on the induced magnetic field signal. This could be attributed to two phenomena. Firstly, the magnetic Reynolds number based on the typical amount of turbulence is very low, giving a very low turbulent magnetic field. Secondly, the size of our magnetic sensor (of order 1 mm^3) acts as a filter for small-scale fluctuations.

The transverse profile of magnetic energy $\langle b_x^2 \rangle$ (figure 13b) is plotted for the same conditions. As expected, we did not observe an induced field for point (i) corresponding
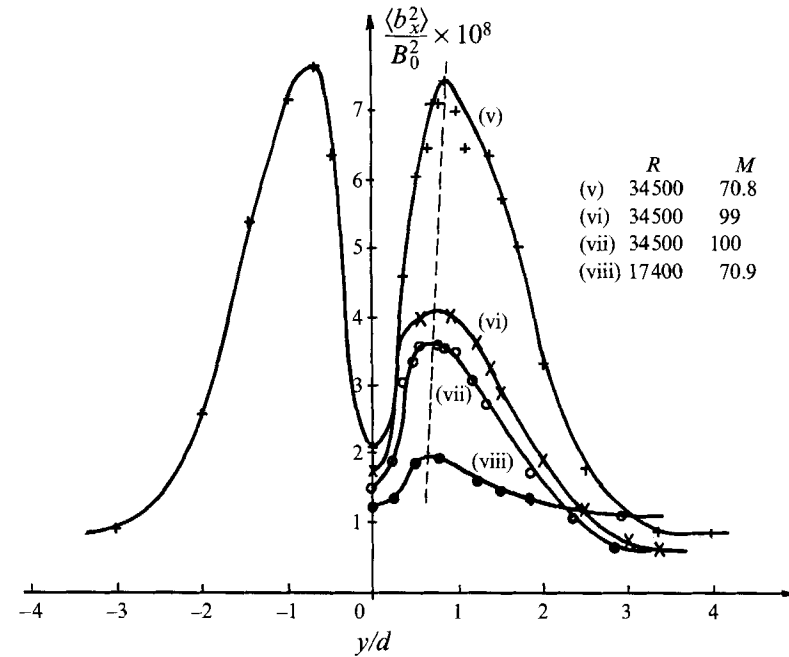
FIGURE 14. Normalized magnetic energy profiles in a cross section located at 2.5 diameters from the cylinder.

to zero external magnetic field. The effect of increasing the Hartmann number is to generate magnetic eddies (in the von Kármán domain) shown on curves corresponding to the points (ii) and (iv). We observe that these two curves are not similar, their shape being a function of the velocity distribution (according to (13)) and consequently of the values M and R. We can also see that increasing the Reynolds number while keeping M constant shifts the peak value from $y/d = 0.75$ (ii) to $y/d = 1$ (iv). This displacement is more important for the magnetic energy distribution than for the kinetic one. This corresponds to the fact that the magnetic eddies can be more elongated than the kinetic ones according to the schematic representation of figure 11. For point (iii), which is outside the von Kármán street region, we observe a flat signal at a low value of induced magnetic field which can be explained as being due to residual turbulence. In this case we also observe an induced magnetic peak near the edge of the cylinder.

The magnetic energy profiles normalized by the square of the external magnetic field intensity (figure 14) confirm the earlier results for higher values of M and R (points (v) and (vi)). The profile obtained for point (viii) is plotted in order to extract the influence of the Reynolds number when M is fixed. For point (v), the measurements were taken for both y positive and y negative in order to verify the symmetry of the magnetic profile. The results show that when M increases, the normalized magnetic energy decreases (because the kinetic energy of the von Kármán street decreases, under the influence of the Joule effect) and the peak of the curves shifts from $y/d = 1$ to $y/d \sim 0.7$. This last point can be explained by two different phenomena which act in the same sense. First, as already noted in the introduction, the boundary-layer separation point is displaced by the magnetic field in the direction of the flow axis downstream, reducing the transverse distance between the two eddy lines in the von Kármán wake. Secondly, it follows from the well-known tendency of the magnetic field

15

to give a two-dimensional flow configuration, that the expansion of the wake decreases when the interaction parameter increases, also reducing the transverse distance between the two eddy lines when x/d increases.

On the other hand, we can observe that when R decreases, the magnetic profile seems to be more elongated in the direction perpendicular to the flow axis (see for example the curve for point (viii) which crosses all the others for large value of y/d). The same observation can be made for the previous results (figure 13b) if using the magnetic curves obtained for points (ii) and (iv). This is due essentially to the normalization of the results using the maximum value of the induced magnetic field as reference (figure 13). The magnetic Reynolds number for curve (iv) is about three times greater than the magnetic Reynolds number for curve (ii) and if we then consider the value of the induced magnetic field without normalization the results for curves (ii) and (iv) are close for $y/d > 2.5$. The residual value can be attributed to the error in the measurement itself. Nevertheless it seems that, even when taking into account the normalization effect, the decrease in the induced magnetic field at large distance y/d is lower for low values of the Reynolds number. The explanation can be attributed to a narrowing of the eddies when one increases the interaction parameter (i.e. R decreases when M is fixed) producing a small elongation of the magnetic lines resulting from a magnetic confinement effect.

On the other hand this narrowing of the eddies when one increases the interaction parameter could also explain the suppression of the von Kármán street. If the distance between eddies becomes too small, some mergings could occur and the detachment from the cylinder could be suppressed. We plan to visualize this evolution by a future free-surface experiment.

The last cross-section profiles considered concern the evolution of the normalized magnetic field for fixed values of the flow parameters M and R when the distance x increases (figure 15a, b). We can see that the peak of the profile has shifted, implying an expansion of the wake, but this expansion is relatively moderate due to the tendency of the applied magnetic field to generate two-dimensionality. We also note that, as expected, the magnetic energy decreases as the distance from the cylinder increases.

3.2.4. *Evolution of the induced magnetic field with Hartmann and Reynolds numbers*

We propose in this last paragraph to complete the main aspects of the characterization of the wake by measuring the evolution of magnetic and kinetic fluctuations at a fixed point with the Hartmann number. We will give, finally, a possible universal representation of the induced magnetic field.

Figure 16(a) represents the evolution of the normalized root-mean-square of the axial velocity fluctuations with the Hartmann number for a given value of the Reynolds number at a fixed distance from the cylinder, $x/d = 2.5$. This evolution has been determined for two characteristic point corresponding to the vicinity of the maximum energy position ($y/d \sim 0.8$) and at the axis of the flow. We establish that for $y/d = 0.8$ the intensity of the velocity fluctuations continuously decreases and reaches a minimum value at a Hartmann number equal to the critical value (cf. figure 8b). On the flow axis this intensity has a relatively high value for $M = 0$ due to the additive effect of the von Kármán eddy fluctuations and turbulence. When the Hartmann number increases, we note an increase in the velocity fluctuations which reach a maximum value for $M \sim 70$. This is surprising because at the same time the velocity decreases at the point $y/d = 0.8$. This phenomenon is because an increase in the magnetic field leads to a decreased distance between the two eddy streets and the influence of each street in the axis becomes more pronounced in spite of the fact that
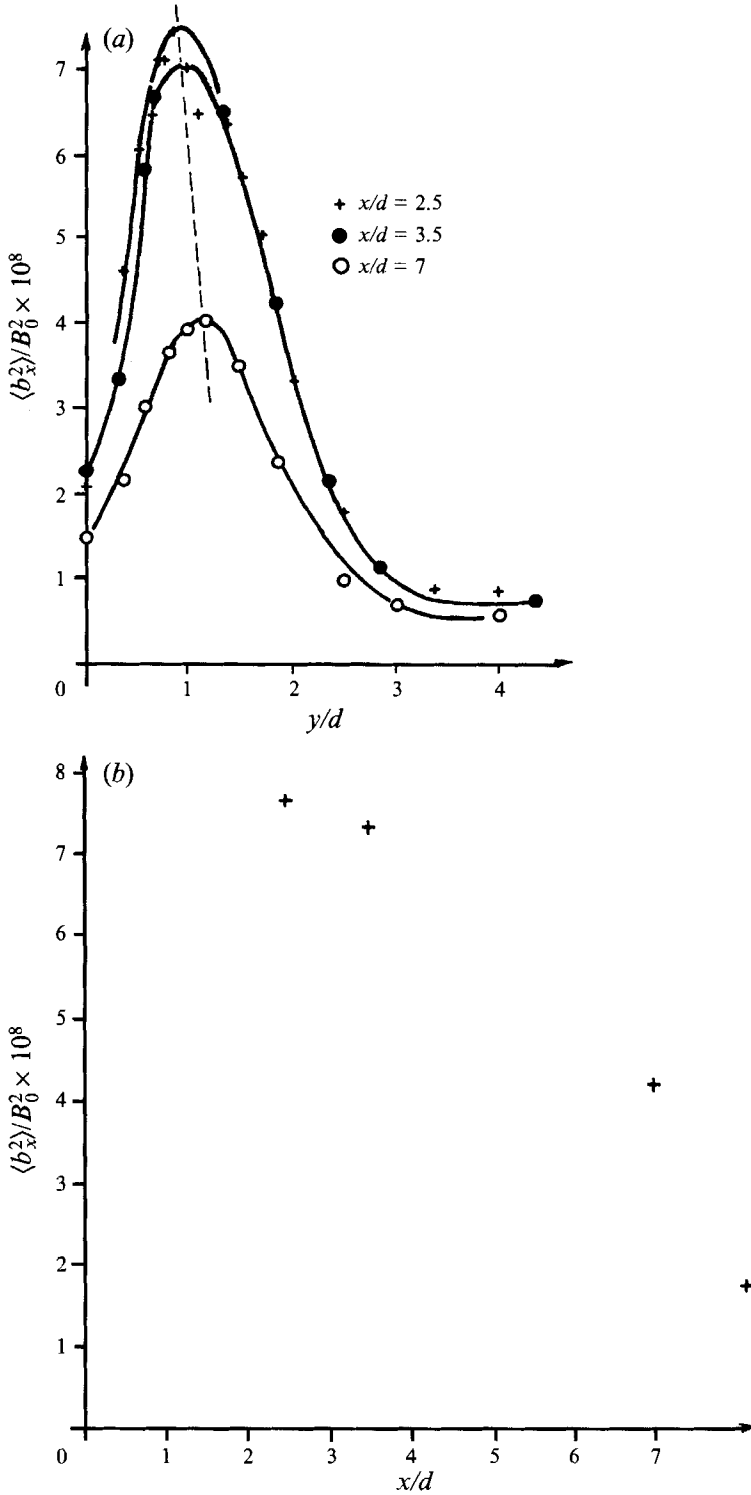
FIGURE 15. Evolution of the normalized magnetic energy with the distance from the cylinder at $R = 34\,500$, $M = 71$, $N = 0.144$.
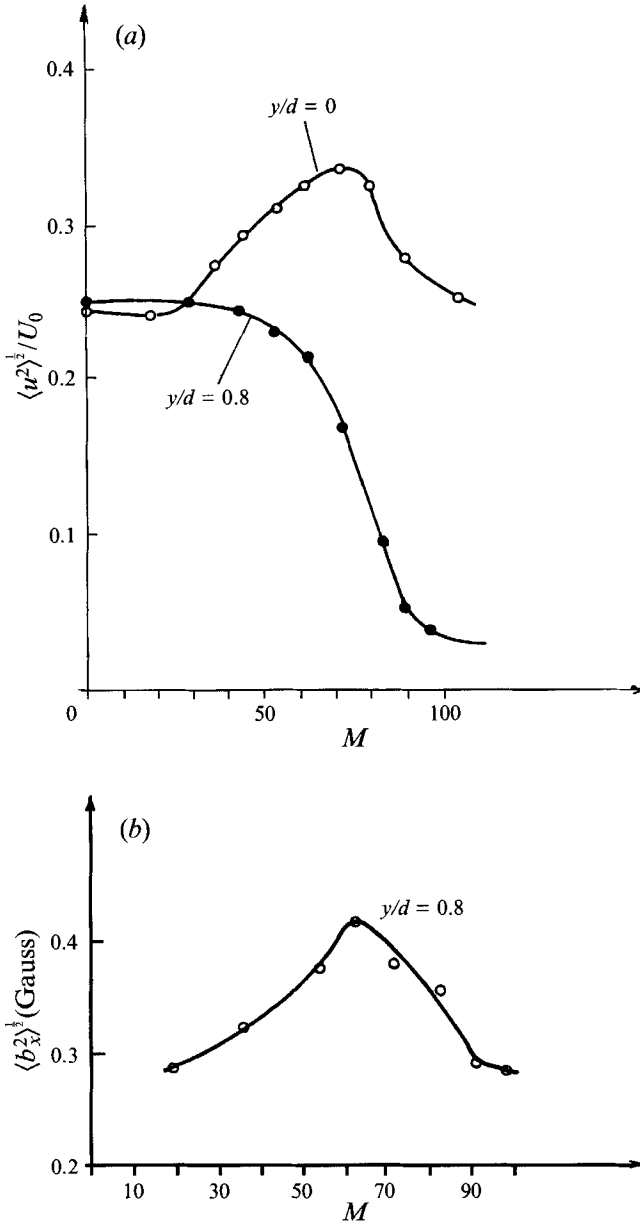
FIGURE 16. (a) Evolution of the normalized kinetic energy at two fixed points with number and (b) evolution of the induced magnetic energy with the Hartmann number, $R = 17400$, $x/d = 2.5$.

a part of the kinetic energy is dissipated by Joule heating. When M increases beyond 70 the velocity intensity decreases (the energy dissipation being a preponderant phenomenon) and reaches a value corresponding to the turbulence intensity alone (as we can see on figure 13 a) for the same critical value of the Hartmann number that we obtained for $y/d = 0.8$.

The evolution of the root mean square of the magnetic fluctuations (figure 16 b) with the Hartmann number, at the same distance from the cylinder ($x/d = 2.5$) and for a given position from the axis ($y/d = 0.8$), can be easily explained by the evolution of the
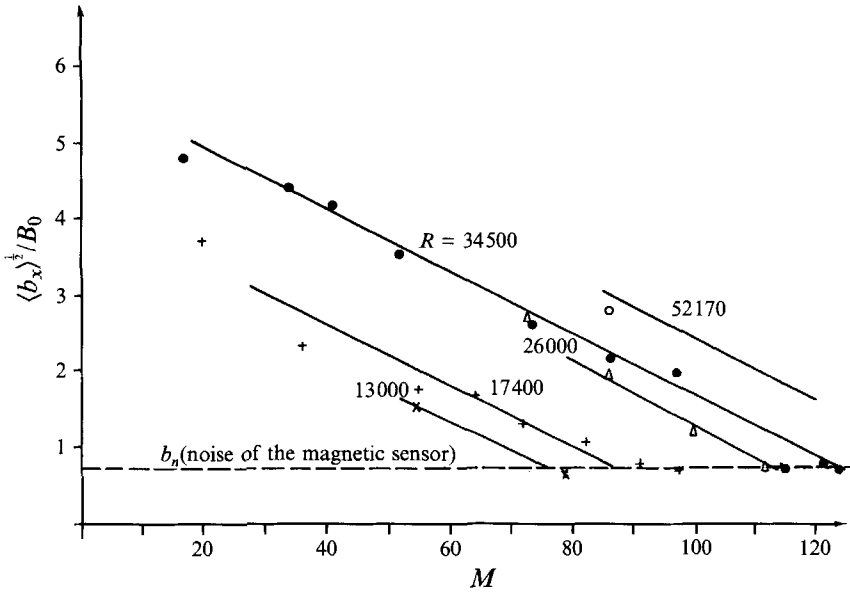
FIGURE 17. Evolution of the root mean square of the induced magnetic field with the Hartmann number, for different values of the Reynolds number at a fixed point $x/d = 2.5$, $y/d = 0.8$.

velocity field. We observe, firstly, an increase in the induced magnetic field when the imposed magnetic field increases. This evolution stays unchanged when the velocity intensity is sufficiently high. The maximum is reached for a Hartmann number equal to 65. Beyond this value, the velocity decreases strongly with M, giving a decrease of the induced magnetic field, which then leads to a constant value for the same critical Hartmann number observed for the velocity evolution. This constant value corresponds to the noise of the probe itself which can be evaluated to an equivalent magnetic intensity of the order of 0.3 Gauss.

To find a universal representation of the evolution of the induced magnetic field taking into account both the Hartmann and Reynolds numbers, we have plotted in figure 17 the evolution of the root-mean-square value of the induced magnetic field normalized by the applied value B_0. For a given value of the Reynolds number (figure 17) the measurement points seem to be organized in parallel straight lines as the Reynolds number changes. The vanishing of the induced magnetic field corresponds, in each case, to the critical Hartmann number M_c according to figure 8(b). A zero induced magnetic field is obtained when the signal reaches the noise value of the magnetodiode called b_n (b_m is the measured induced magnetic field). Then we can conclude that, plotting the quantity $(b_m - b_n)$ as a function of $(M - M_c)$ gives a single universal straight line (figure 18). If the critical Hartmann number is given by $N = 0.55$ ($M_c^2/R = 0.55$) the universal law takes the form

$$\frac{\langle b^2 \rangle^{\frac{1}{2}}}{B_0} = \alpha[(0.55R)^{\frac{1}{2}} - M]\, h\!\left(\frac{y}{d}, \frac{x}{d}\right),$$

where, according to figure 18 α is equal to 4.75×10^{-6}. The function $h(y/d, x/d)$ characterizes the measurement point and is finally equal to one (by definition) for our experimental conditions.
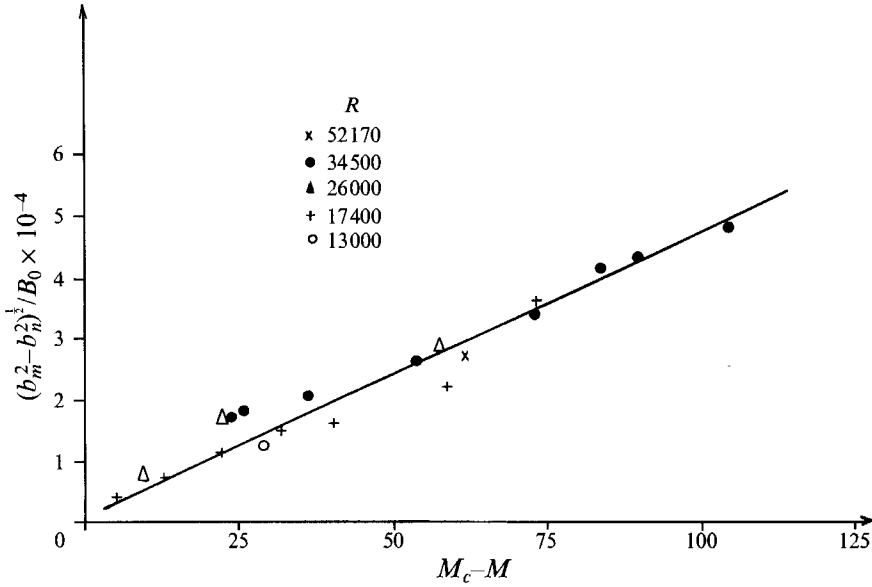
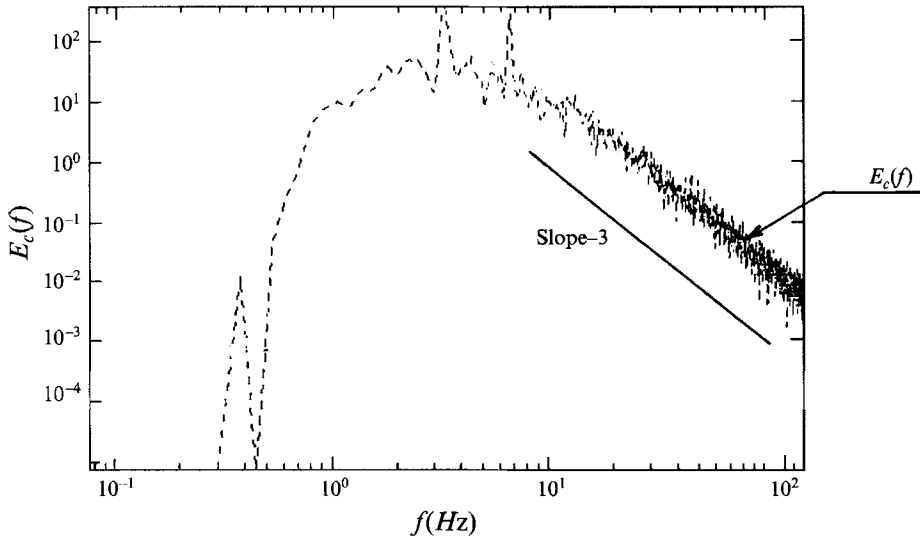FIGURE 18. Universal evolution of the root mean square of the induced magnetic field with the Hartmann number.

FIGURE 19. Energy spectrum of the velocity fluctuation downstream of the cylinder for $y/d = 0$ and $x/d = 2.5$.

3.2.5. Spectral analysis

A short spectral analysis of the velocity field on the axis of the flow downstream from the cylinder, for experimental conditions corresponding to a strong influence of the external magnetic field on the von Kármán eddies, is shown on figure 19. Here the kinetic energy spectrum exhibits a k^{-3} law. One possible explanation of these results is that, due to the influence of the external magnetic field, the flow configuration is stabilized in a nearly two-dimensional configuration. Then the von Kármán eddies, which give a frequency readily observed on the energy spectrum, appears as an

external forcing on two-dimensional turbulence, which then results in an enstrophy cascade characterized by the well-known k^{-3} law. Such a law, also observed in homogeneous MHD turbulence (Alemany *et al.* 1979; Caperan & Alemany 1985), was explained in this case by a quasi-equilibrium between Joule effect and angular energy transfer in Fourier space.

4. Conclusion

We have presented an experimental analysis of both the upstream and downstream wakes of a cylinder in a conducting fluid which has been subjected to an external, aligned magnetic field. Upstream, the measurements confirm the existence of a wake and give the influence of the blockage ratio on the evolution of the magnetic and kinetic perturbations. Downstream from the cylinder, the main result concerns the suppression of the von Kármán eddies which seems to occur at a critical interaction parameter of approximately 0.5. This phenomena could be explained by a narrowing of the eddies, when the interaction parameter increases, producing some joining between them, and at the end suppressing the detachment from the cylinder. The experimental analysis of this transition merits further study.

REFERENCES

AHLSTROM, M. G. 1963 Experiments on the upstream wake in magneto-fluid dynamics. *J. Fluid Mech.* **15**, 205–222.

ALEMANY, A., MOREAU, R., SULEM, P. L. & FRISCH, U. 1979 Influence of an external magnetic field on homogeneous M.H.D. turbulence. *J. Méc.* **18**, 277–313.

BORISOV, B. P. & KRASILNIKOVE, J. 1981 Experimental determination of the condition for unseparated flow behind a cylinder in a longitudinal magnetic field. *Proc. Riga Sem. on MHD*, pp. 57–58 (in Russian).

CAPERAN, PH. & ALEMANY, A. 1985 Turbulence homogène MHD à faible nombre de Reynolds magnétiques. Etude de la transition vers la phase quasi bidimensionalle et caractérisation de son anisotropie. *J. Méc. Théror. Appl.* **4**, 175–200.

CRISTOLOVEANU, S. 1981 Transport magnétoélectrique dans les semi-conducteurs en présence d'inhomogénéités naturelles ou induites par effet de recombinaison et d'injection. Application aux capteurs magnétiques. Doctorat d'Etat. Université Scientifique et Médicale de Grenoble et Institut National Polytechnique de Grenoble.

GOLUBJEV, A. V., KASCHULIN, A. P., KRASILNIKOVE, J. & LUSCHIK, W. G. 1984 Flow of liquid metal around a cylinder in a longitudinal magnetic field. *Proc. MHD Conf. Riga*, pp. 95–98 (in Russian).

HORLOCK, J. H. 1963 Some two-dimensional magneto-fluid dynamic flow at low magnetic Reynolds number. *J. Fluid Mech.* **16**, 17–33.

JOSSERAND, J., MARTY, PH. & ALEMANY, A. 1993 Pressure and drag measurements on a cylinder in a liquid metal flow with an aligned magnetic field. *Fluid Dyn. Res.* **11**, 107–117.

LAHJOMRI, J. 1988 Caractérisation de la structure de sillages M.H.D. amont et aval d'un cylindre à petit nombre de Reynolds magnétiques. Thèse de l'Université Joseph Fourier-Grenoble 1.

LAKE, B. M. 1971 Velocity measurements in region of upstream influence of a body in aligned-fields MHD flow. *J. Fluid Mech.* **50**, 209–231.

MAXWORTHY, T. 1962 Measurements of drag and wake structure in magneto fluid dynamic flow about a sphere. *Proc. Heat Trans. Fluid Mech. Inst. Seattle, WA, June 13–15, 1962*, pp. 197–204. Stanford University Press.

MAXWORTHY, T. 1968 Experimental studies in magneto-fluid dynamics: pressure distribution measurements around a sphere. *J. Fluid Mech.* **31**, 801–814.

MAXWORTHY, T. 1969 Experimental studies in magneto-fluid dynamics: flow over a sphere with cylindrical after body. *J. Fluid Mech.* **35**, 411–416.

ROSHKO, A. 1954 On the development of the turbulent wakes from vortex streets. *Natl Adv. Comm. Aero., WA Rep.* 1197.

SHERCLIFF, J. A. 1965 *A Textbook of Magnetohydrodynamics.* Pergamon.

TAMADA, K. 1962 Flow of slightly conducting fluid past a circular cylinder with strong aligned magnetic field. *Phys. Fluids* **5**, 817–823.

YONAS, G. 1967 Measurements of drag in a conducting fluid with an aligned field and large interaction parameter. *J. Fluid Mech.* **30**, 813–821.

YOSINOBU, H. 1960 A linearized theory of magnetodynamic flow past a fixed body in parallel magnetic field. *J. Phys. Soc. Japan* **15**, 175–188.